Ligand and Structure-Based Virtual Screening in Combination, to Evaluate Small Organic Molecules as Inhibitors for the XIAP Anti-apoptotic Protein: The Xanthohumol Hypothesis.

Aggeliki Mavra, Christos C. Petrou and Manos C. Vlasiou*

vlasiou.m@unic.ac.cy

Keywords: Molecular docking, molecular dynamics, pharmacophore, molecular modeling, XIAP protein, protein inhibitor, anticancer activity.

Abstract

Herein, we are proposing two chalcone molecules, (E)-1-(4-methoxyphenyl)-3-(p-tolyl) prop-2-en-1-one and (E)-3-(4-hydroxyphenyl)-1-(2,4,6-trihydroxyphenyl) prop-2-en-1-one, based on the anticancer bioactive molecule Xanthohumol, which are suitable for further *in vitro* and *in vivo* studies. Their ability to create stable complexes with the antiapoptotic X-linked IAP (XIAP) protein makes them promising anticancer agents. The calculations were based on ligand-based and structure-based virtual screening combined for the pharmacophore built. Additionally, the structures passed Lipinski's rule for drug use, and their reactivity was confirmed using density functional theory studies. The candidates were chosen between 10639400 compounds, and the docking protocols were evaluated using molecular dynamics simulations.

1. Introduction

In the last decades, researchers have received much attention on the antitumor effect of the prenylated chalcone called Xanthohumol (XN). More specifically, the anticancer activity of this molecule has been marked by intracellular ROS induction, endoplasmic reticulum stress induction, and disruption of the BIG3-PHB2 interaction [1]. BIG3-PHB2 interaction happens between the A-inhibited guanine nucleotide-exchange protein 3 (BIG3) and prohibitin 2 (PHB2) in the cytoplasm of breast cancer cells [2,3]. Additionally, XN inhibits DNA synthesis, arresting the cancer cell cycle at the S phase [4]. The chemical structure of this flavonoid consists of trans-configured A, and B aromatic rings joined through a three-carbon, unsaturated carbonyl system substituted by hydroxyl groups, a methoxy group, and a prenyl unit [5].

Programmed cell death is one of the most common cancer therapies in tumor cells. Defections of the pro-apoptotic death regulators, such as BH3-only proteins, cause chemotherapy failure [6]. Inhibition of apoptosis proteins (IAP) through apoptosis regulators is characterized by the presence of three domains known as baculoviral IAP repeat (BIR) domains [7,8]. Among these

Preprints (www.preprints.org) | NOT PEER-REVIEWED | Posted: 9 June 2022 doi:10.20944/preprints202206.0144.v1

IAP proteins, cellular IAP-1 (cIAP-1) and cIAP-2 play a critical role in the regulation of tumor necrosis factor (TNF) receptor-mediated apoptosis, while X-linked IAP (XIAP) is a central regulator of both deaths' receptor-mediated and mitochondria-mediated apoptosis pathways [9]. XIAP inhibits apoptosis by suppressing caspase activity, whereas the third BIR domain (BIR3) of XIAP selectively targets an initiator caspase-9, the BIR2 domain, and the linker immediately preceding it, inhibits effector caspase-3/caspase-7. XIAP and cIAP-1 were highly expressed in cancers of diverse tumor types and are considered attractive cancer therapeutic targets [10,11].

Structure-based pharmacophore (SBP) design and hybrid virtual screening protocol can be used to detect novel Xanthohumol-based lead compounds based on changes in the chemical scaffold [12]. Pharmacophore query is widely applied in database screening. As far as now, the ligand-based pharmacophore model has been utilized frequently. Nowadays, with large numbers of protein structures being elucidated, the application of structure-based pharmacophore has obtained more popularity [13]. Combining two pharmacophore generation strategies has already become the mainstream in computer-aided virtual screening. Moreover, computational approaches like molecular dynamics simulations, molecular docking, drugs-likeness prediction, *and in silico* ADMET study are adopted mainly to screen potential drugs/molecules from various databases/libraries, saving experimental cost and time in drug discovery [14,15].

Starting from the Xanthohumol molecule and its proven anticancer activity from the literature [16-20], we performed virtual screening, ligand (ligand similarity), and structurally based (ligand docking on XIAP protein) screening. After building our pharmacophore model, molecular dynamics evaluated the docking protocol. The best candidate molecules were also assessed through ADMET predictions to confirm their pharmacological use and quantum chemistry to evaluate their reactivity.

2. Computational Methods

After concluding from the literature on the proven anticancer activity of Xanthohumol, we followed two approaches regarding the virtual screening procedure. First, using SMILES chemical format to describe the structure of the starting molecule, we performed ligand-based screening similarity using the SwissSimilarity Webserver (http://www.swisssimilarity.ch/). Through the available screening libraries, we have chosen ''ZINC drug'' (a library of 10639400 structures) and, for the screening method, the "pharmacophore" built. This procedure

 doi:10.20944/preprints202206.0144.v1

gave us 400 candidate molecules. On the same server, (SwissADME) pharmacokinetic properties evaluation, physicochemical properties, and drug-likeness were performed [21]. This procedure minimized the number of candidate molecules. Sixty-two candidate molecules had the characteristics to be considered as drugs based on our first structure (Xanthohumol). To further reduce the number of the candidate molecules, structure-based screening was performed using AutoDock Vina (https://autodock.scripps.edu). Docking was carried out on PyRx using the AutoDock Vina option and ran at an 'exhaustiveness' of 8. The grid box was centered at X=12.1477, Y=–3.5864, Z=18.4151, with a grid dimension of 45.0279 Å x 68.7439 Å x 56.9456 Å, thereby enclosing the active site residues and the binding site as well. Following a series of ligand-receptor docking runs, Vina evaluates the results, calculates the binding affinities of the ligands, and clusters the resulting poses based on their conformational overlaps. After choosing the best pose from each group, the ligands are ranked according to their binding affinities [22]. According to their binding affinities, the docking results of the top ligands were first validated by re-docking them into the same defined regions of the receptor using AutoDock Vina. The re-docked complex was superimposed on the reference co-crystallized complex, and the root means square deviation (RMSD) was calculated.

Additionally, molecular dynamics simulations were performed as a second validation method, using the AMBER force fields [23]. The complexes were placed in a rectangular parallelepiped water box, and an explicit solvent model for water was used while the complexes were solvated with 10-Å water cap. Chlorine ions were added as counterions to neutralize the system. Before MD simulations, one step of minimization was carried out. Particle mesh Ewald electrostatics and periodic boundary conditions were used in the simulation [24]. The MD trajectories were run using the minimized structures as the starting conformations. The time step of the simulations was 2.0 fs with a cutoff of 10 Å for the non-bonded interaction. Constant-volume periodic boundary MD was carried out for 300 ps. The temperature was raised from 0 to 300 K. Then, 1.7 ns of constant pressure irregular boundary MD was carried out at 300 K using the Langevin thermostat to maintain the temperature of our system constant. The ligand's disposition was monitored. All ligands that showed an average RMSD greater than 2 Å concerning the reference disposition were discarded using the docking result as a reference pose.

The structure-based pharmacophore modeling was performed by molecular docking using the iGEMDOCK software [25]. The 5OQW coded crystal structure of XIAP protein was selected from the Protein Data Bank (www.rcsb.org). Ligand molecules (the best candidates with higher

Preprints (www.preprints.org) | NOT PEER-REVIEWED | Posted: 9 June 2022 doi:10.20944/preprints202206.0144.v1

binding affinities) were collected by Drug Bank (www.drugbank.ca). Ligand molecules included the Xanthohumol molecule used for the pharmacophore modeling. The protein structure was then prepared by assigning the hydrogen atoms, charges, and energy minimization using CHIMERA software [26]. The energy minimization was performed using 500 steepest descent steps with 0.02 Å step size and an update interval of 10. Before completing the molecular docking of ligand and receptor, the ligands were optimized by adding hydrogens using CHIMERA software. Using ORCA, DFT studies obtained the optimized structures under the B3LYP/6 311++G (d, p) level of theory [27-29]. The scoring function consisted of a simple empirical scoring function and a pharmacophore-based scoring function to reduce the number of false positives. The energy function can be dissected into the following terms:

$$E_{tot} = E_{bind} + E_{pharma} + E_{ligpre} \quad (1)$$

E_{bind} is the empirical binding energy used during molecular docking; E_{pharma} is the energy of binding-site pharmacophores; E_{ligpre} is a penalty value if the ligand is unsatisfied with the ligand preferences. E_{pharma} and E_{ligpre} were used to improve the number of true positives. The empirical binding energy (E_{bind}) is given as:

$$E_{bind} = E_{inter} + E_{intra} + E_{penal} \quad (2)$$

E_{inter} and E_{intra} are intermolecular and intramolecular energy, respectively. E_{penal} is a large penalty value if the ligand is out of the range of the search box. In this paper, E_{penal} is set to 10000. For screening: The population size was = 200, generations = 70, number of solutions = 3. Fitness is the total energy of a predicted pose in the binding site. The empirical scoring function of iGEMDOCK is estimated as:

$$\text{Fitness} = \text{vdW} + H_{bond} + \text{Elec.} \quad (3)$$

Here, the vdW term is van der Waals energy. H_{bond} and Elect terms are hydrogen bonding energy and electrostatic energy, respectively—screenshots of the ligand-amino acid residue interactions created by CHIMERA software. The docking results of the ligands were validated by re-docking them into the same defined regions of the receptor using the crystalized structure.

3. Results and Discussion

After a literature search regarding the *in vitro* and *in vivo* anticancer activity of Xanthohumol, we realized that there was not any *in silico* procedure that evaluates or further studies this specific hypothesis. This prenylated chalcone provides a scaffold for other chalcone derivatives with the same or better anticancer activity. To check that, using the Swiss Institute of Bioinformatics server, we managed to find, based on this virtual ligand screening, that 10639400 similar structures could provide the same activity (SwissSimilarity). To minimize the number of the candidate molecules, ADMET studies with the help of the same server gave 400 that could be used as drugs. Additionally, these molecules can interact based on their chemical structure with the protein 5-lipoxygenase (SwissTargetPrediction) (2Q7R code for crystal structure in Protein Data Bank). Surprisingly, XIAP protein was not a candidate structure to interact with none of these molecules. XIAP is an antiapoptotic protein, and we believe that inhibition of this protein could induce anticancer activity. Furthermore, structure-based virtual screening was followed for these two protein structures (2Q7R and 5OQW). The ligands were the 400 candidate molecules derived after ADMET studies. Sixty-two of these molecules, based on their binding affinities (with 5-lipoxygenase) after docking studies, were used in further docking studies with the XIAP protein (5OQW). The docking results were evaluated with the methods described above in computational methods. The complete flowchart of the work can be seen in **Figure 1**. The two best candidate molecules (E)-1-(4-methoxyphenyl)-3-(p-tolyl) prop-2-en-1-one (MW: 252.31) **(A)** and (E)-3-(4-hydroxyphenyl)-1-(2,4,6-trihydroxyphenyl) prop-2-en-1-one (MW: 272.25) **(B)** are depicted in **Figure 2**. After evaluating the docking protocol, the two molecules were selected (RMSD value < 2 Å). Docking validation RMSD values can be found in supplementary **SFigure 1**. Density functional theory studies on B3LYP/6 311++G (d, p) level of theory has performed to discriminate the chemical reactivity between (E)-1-(4-methoxyphenyl)-3-(p-tolyl) prop-2-en-1-one and (E)-3-(4-hydroxyphenyl)-1-(2,4,6-trihydroxyphenyl) prop-2-en-1-one. We were able to calculate the molecular orbitals of the two molecules as well. The value of the energy difference between HOMO and LUMO and the highest occupied molecular orbital (EHOMO) and lowest unoccupied molecular orbital (ELUMO) energies play a significant role in the stability and reactivity of molecules. The EHOMO energies of molecules show the molecule's ability to give electrons. On the other hand, ELUMO characterizes the ability of the compound to accept electrons. Electronegativity (χ) measures an atom's power to attract a bonding pair of

Preprints (www.preprints.org) | NOT PEER-REVIEWED | Posted: 9 June 2022 doi:10.20944/preprints202206.0144.v1

electrons. Based on equation χ = - (EHOMO + ELUMO)/2, a larger Δgap always indicates lower chemical reactivity and higher kinetic stability of the investigated species. The simultaneous effect of different parameters causes the chemical reactivity of molecules. The distribution and energy of HOMO are important parameters to explain the antioxidant potential of phenolic antioxidants. The electron-donating capacity of the molecule can be predicted by looking at the energy values of HOMO. The value of the energy difference between HOMO and LUMO, as well as the highest occupied molecular orbital (EHOMO) and lowest unoccupied molecular orbital (ELUMO) energies, plays a critical role in stability and reactivity [30, 31]. In particular, in the first candidate, the LUMO orbital equals -6.243 eV while the HOMO orbital equals -11.202 eV. On the other hand, regarding the second molecule, the LUMO orbital equals -5.487 eV, and the HOMO orbital equals -10.855 eV. Based on that, the **B** molecule is more electronegative than the **A** (larger Δgap). The quantum chemical descriptors of the molecules can be found in **Table 1**. The results show that (E)-3-(4-hydroxyphenyl)-1-(2,4,6-trihydroxyphenyl) prop-2-en-1-one has higher reactivity based on the calculated energy gap of HOMO and LUMO orbitals. These results are in agreement with the docking work. The docking results show that (E)-3-(4-hydroxyphenyl)-1-(2,4,6-trihydroxyphenyl) prop-2-en-1-one has better binding affinity amongst the best two candidates (-72.13 Kj/mol). Specifically, molecule **A** has a binding affinity of -69.10 kJ/mol with the target protein. Additionally, this energy corresponds only to van der Waals interactions since the molecule has no hydrogen bond with the amino acid pocket. The amino acid residue of the protein that interacts with molecule **A** is Leu 307, Thr 308, Trp 310, Glu 314, Gln 319, Trp 323, and Tyr 324. Molecule **B** interacts with three hydrogen bonds with Ser 278, Val 279, Trp 310 (Energy contribution, -12.08 Kj/mol) and has van der Waals interactions with Val 279, Gly 293, Glu 294, Asp 296, Trp 310 (Energy contribution -62.05 Kj/mol). The total binding affinity of the **B** molecule with the XIAP protein is -74.13 Kj/mol. Docking results can be found in **Table 2**. Additionally, the binding position of the best conformations on XIAP protein can be seen in **Figure 3**. Here, we can see that the conformations of the best candidates interact with the binding pocket of XIAP protein. **In Figure 4,** we can see the detailed interaction of the amino acid residues of XIAP protein with (E)-1-(4-methoxyphenyl)-3-(p-tolyl) prop-2-en-1-one and (E)-3-(4-hydroxyphenyl)-1-(2,4,6-trihydroxyphenyl) prop-2-en-1-one. ADME studies repeated in particular for (E)-3-(4-hydroxyphenyl)-1-(2,4,6-trihydroxyphenyl) prop-2-en-1-one since it has the best binding affinity with the protein and the results are depicted on **Table 3**. The best candidate (Molecule **B**), in total, has 20 heavy atoms (none hydrogen atoms) and three rotatable bonds. The important aspect is that it has five hydrogen bond acceptors and four hydrogen bond

Preprints (www.preprints.org) | NOT PEER-REVIEWED | Posted: 9 June 2022 doi:10.20944/preprints202206.0144.v1

donors. The interaction with XIAP protein created three hydrogen bonds with the amino acids Ser 278, Val 279, and Trp 310. It passes all Lipinski's rules to be regarded as a drug and does not penetrate the blood-brain barrier, an important aspect of it is future use as an anticancer agent. Finally, the pharmacophore descriptors, hydrogen donor atoms, and hydrogen acceptor atoms can be found in **Figure 5**, while details about the radius and coordinates are supplementary on **Stable 1**. Specifically, we can observe the positions of the molecules that are responsible for hydrogen bonding with the XIAP protein and the areas responsible for the van der Waals interactions. After using ligand and structure-based virtual screening, we present two possible candidates based on the prenylated chalcone Xanthohumol and the X-linked IAP antiapoptotic protein. The ((E)-1-(4-methoxyphenyl)-3-(p-tolyl) prop-2-en-1-one and the (E)-3-(4-hydroxyphenyl)-1-(2,4,6-trihydroxyphenyl) prop-2-en-1-one), that can be considered in further anticancer *in vitro* and *in vitro studies*. The use of quantum chemistry through density functional theory studies showed evidence of higher reactivity of (E)-3-(4-hydroxyphenyl)-1-(2,4,6-trihydroxyphenyl) prop-2-en-1-one), the fact that it is in agreement with the better free Gibb’s energy of the stable complex with XIAP protein.

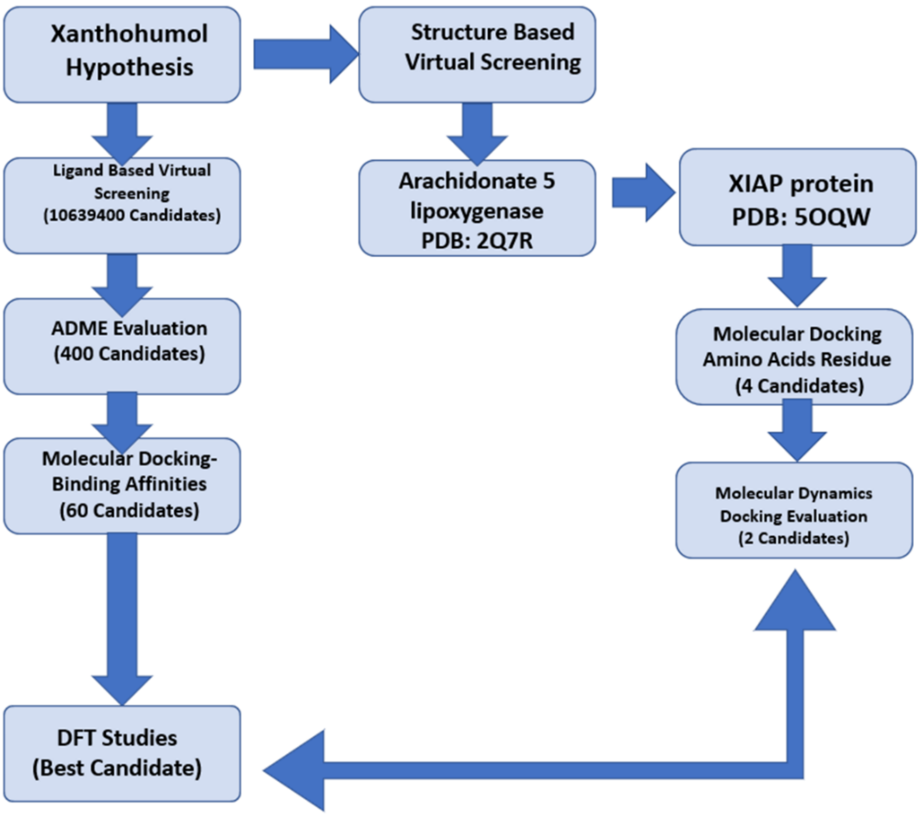

Figure 1: Workflow of the study.

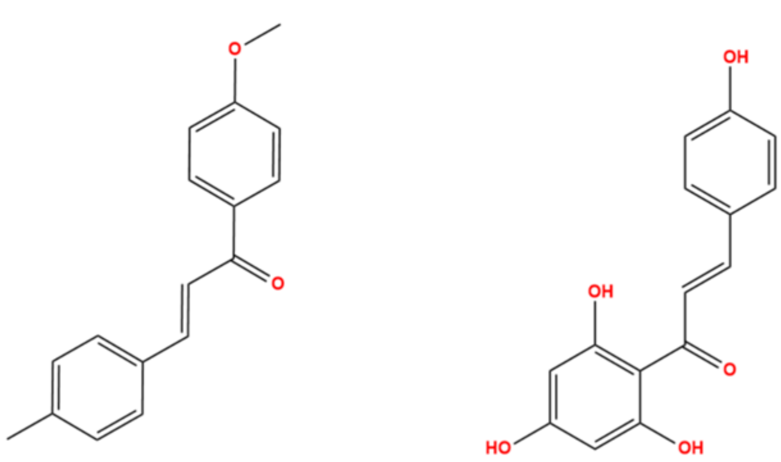

(E)-1-(4-methoxyphenyl)-3-(p-tolyl)prop-2-en-1-one (MW: 252.31)

(E)-3-(4-hydroxyphenyl)-1-(2,4,6-trihydroxyphenyl)prop-2-en-1-one (MW: 272.25)

Figure 2: Candidate molecules.

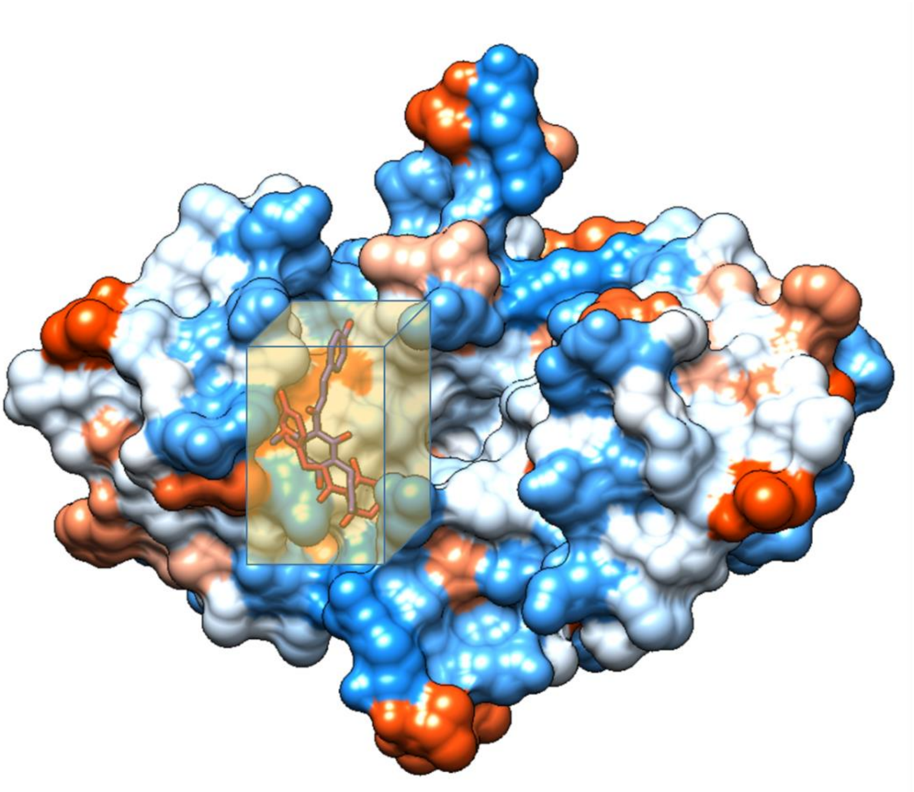

Figure 3: Binding pocket of XIAP protein.

Preprints (www.preprints.org) | NOT PEER-REVIEWED | Posted: 9 June 2022 doi:10.20944/preprints202206.0144.v1

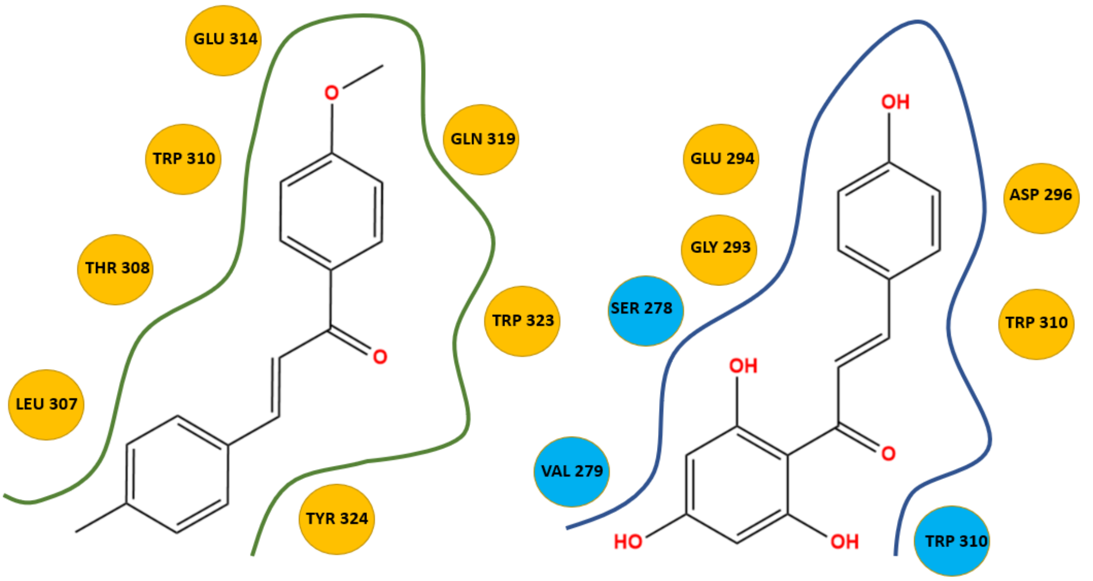

(E)-1-(4-methoxyphenyl)-3-(p-tolyl)prop-2-en-1-one (MW: 252.31)

(E)-3-(4-hydroxyphenyl)-1-(2,4,6-trihydroxyphenyl)prop-2-en-1-one (MW: 272.25)

Figure 4: Amino acid residue of XIAP protein interacting with the two molecules (Blue color: H-bonds).

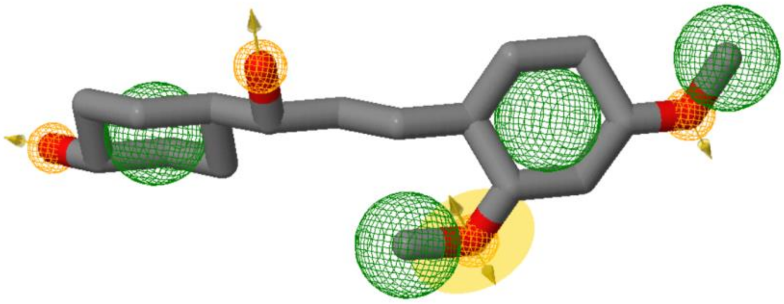

Figure 5: Pharmacophore descriptors.

Preprints (www.preprints.org) | NOT PEER-REVIEWED | Posted: 9 June 2022 doi:10.20944/preprints202206.0144.v1

Table 1: Quantum chemical descriptor of the best candidates calculated by density functional theory study.

Quantum Chemical Descriptor	(E)-1-(4-methoxyphenyl)-3-(p-tolyl) prop-2-en-1-one	(E)-3-(4-hydroxyphenyl)-1-(2,4,6-trihydroxyphenyl) prop-2-en-1-one
μ	-8.723 eV	-8.171 eV
n	4.959 eV	5.386 eV
I	11.202 eV	10.855 eV
A	6.243 eV	5.487 eV
ω	7.672 eV	6.198 eV
χ	8.732 eV	8.171 eV
ζ	0.202 eV	0.186 eV
E_{gap}	4.959 eV	5.386 eV

Table 2: Energies and amino acid residue of the best two candidates on XIAP protein.

Complex	Total Energy (KJ/mole)	Energy H_{Bond} (KJ/mole)	Energy VDW (KJ/mole)	Amino Acid Residue H_{Bond}	Amino Acid Residue VDW Interactions
A-5OQW	-69.10	0	-69.10	None	Leu 307, Thr 308, Trp 310, Glu 314, Gln 319, Trp 323, Tyr 324
B-5OQW	-74.13	-12.08	-62.05	Ser 278, Val 279, Trp 310	Val 279, Gly 293, Glu 294, Asp 296, Trp 310

Table 3: ADME studies of OC1=CC=C(C=C1)/C=C/C(=O)C2=C(O)C=C(O)C=C2O input.

ADME Characteristics	Value-Answer
Formula	$C_{15}H_{12}O_5$
Molecular weight	272.25 g/mol
Number of heavy atoms	20
Number of rotatable bonds	3
Number of Hydrogen bond acceptors	5
Number of Hydrogen bond donors	4
Molar refractivity	74.34
Log $P_{o/w}$	1.90
Log S	-3.55
GI absorption	High
BBB permeant	No
CYP1A2 Inhibitor	Yes
CYP2C19 Inhibitor	No
CYP2C9	Yes
CYP2D6	No
CYP3A4	Yes
Log Kp	-5.96 cm/s
Lipinski	Yes, 0 violation
Bioavailability Score	0.55
Leadlikeneness	Yes
Synthetic accessibility	2.56

Conclusions

Based on computer-aided drug discovery (CADD) calculations, we have predicted two chalcone molecules that are good candidates to be evaluated as inhibitors for the antiapoptotic protein XIAP. The calculations provide new insights into anticancer drug discovery since XIAP is highly expressed in cancers of diverse tumor types and is considered an attractive therapeutic target. We have built our pharmacophore model based on the Xanthohumol hypothesis. XN is a biomolecule with proven *in vitro* and *in vivo* anticancer activity, and we have run ligand-based and structure-based virtual screening. Starting from 10639400 structures we concluded that ((E)-1-(4-methoxyphenyl)-3-(p-tolyl) prop-2-en-1-one and (E)-3-(4-hydroxyphenyl)-1-(2,4,6-trihydroxyphenyl) prop-2-en-1-one) are the best candidates. Moreover, quantum chemical descriptors help us understand and discriminate the second molecule as a better structure relying on its higher chemical activity. (E)-3-(4-hydroxyphenyl)-1-(2,4,6-trihydroxyphenyl) prop-2-en-1-one) has passed the Lipinski's rule for drugs; it has five hydrogen acceptor atoms and four hydrogen donor atoms, makes it easy to create hydrogen bonds with the amino acids Ser 278, Val 279, Trp 310 of XIAP binding pocket.

 doi:10.20944/preprints202206.0144.v1

Author Contributions

Conceptualization, M.C.V.; methodology, M.C.V.; software, C.C.P..; validation, M.C.V., resources, C.C.P.; writing—original draft preparation, A.M.; writing—review and editing, M.C.V.; visualization, M.C.V.; supervision, M.C.V. All authors have read and agreed to the published version of the manuscript.

Funding

This research received no external funding.

Data Availability Statement

Not applicable.

Conflicts of Interest

The authors declare no conflict of interest.

References:

[1] Y. Shikata, T. Yoshimaru, M. Komatsu, H. Katoh, R. Sato, S. Kanagaki, Y. Okazaki, S. Toyokuni, E. Tashiro, S. Ishikawa, T. Katagiri, M. Imoto, Protein kinase A inhibition facilitates the antitumor activity of xanthohumol, a valosin-containing protein inhibitor, Cancer Sci. 108 (2017) 785–794. https://doi.org/10.1111/cas.13175.

[2] T. Yoshimaru, M. Komatsu, T. Matsuo, Y.A. Chen, Y. Murakami, K. Mizuguchi, E. Mizohata, T. Inoue, M. Akiyama, R. Yamaguchi, S. Imoto, S. Miyano, Y. Miyoshi, M. Sasa, Y. Nakamura, T. Katagiri, Targeting BIG3-PHB2 interaction to overcome tamoxifen resistance in breast cancer cells, Nat. Commun. 4 (2013) 4–7. https://doi.org/10.1038/ncomms3443.

[3] T. Yoshimaru, M. Komatsu, E. Tashiro, M. Imoto, H. Osada, Y. Miyoshi, J. Honda, M. Sasa, T. Katagiri, Xanthohumol suppresses estrogen-signaling in breast cancer through the inhibition of BIG3-PHB2 interactions, Sci. Rep. 4 (2014) 1–9. https://doi.org/10.1038/srep07355.

[4] V. Harish, E. Haque, M. Śmiech, H. Taniguchi, S. Jamieson, D. Tewari, A. Bishayee, Xanthohumol for human malignancies: Chemistry, pharmacokinetics and molecular targets, Int. J. Mol. Sci. 22 (2021). https://doi.org/10.3390/ijms22094478.

[5] M.C. Vlasiou, C.C. Petrou, Y. Sarigiannis, K.S. Pafiti, Density functional theory studies and molecular docking on xanthohumol, 8-prenylnaringenin and their symmetric substitute diethanolamine derivatives as inhibitors for colon cancer-related proteins, Symmetry (Basel). 13 (2021). https://doi.org/10.3390/sym13060948.

[6] P. Obexer, M. Ausserlechner, X-linked inhibitor of apoptosis (XIAP) - a critical death-resistance regulator and therapeutic target for personalized cancer therapy, Front. Oncol. 4 JUL (2014) 1–9. https://doi.org/10.3389/fonc.2014.00197.

[7] M.M. Wilson, M.S., Metink-Kane, 基因的改变NIH Public Access, Bone. 23 (2012) 1–7. https://doi.org/10.1016/j.bmcl.2013.04.096.Design.

[8] C. Lukacs, C. Belunis, R. Crowther, W. Danho, L. Gao, B. Goggin, C.A. Janson, S. Li, S. Remiszewski, A. Schutt, M.K. Thakur, S.K. Singh, S. Swaminathan, R. Pandey, R. Tyagi, R. Gosu, A. V. Kamath, A. Kuglstatter, The structure of XIAP BIR2: Understanding the selectivity of the BIR domains, Acta Crystallogr. Sect. D Biol. Crystallogr. 69 (2013) 1717–1725. https://doi.org/10.1107/S0907444913016284.

[9] J. Lu, L. Bai, H. Sun, Z. Nikolovska-coleska, S. Qiu, R.S. Miller, H. Yi, S. Shangary, Y. Sun, J.L. Meagher, J.A. Stuckey, S. Wang, NIH Public Access, 68 (2009) 9384–9393. https://doi.org/10.1158/0008-5472.CAN-08-2655.SM-164.

[10] Y. Nakagawa, S. Abe, M. Kurata, M. Hasegawa, K. Yamamoto, M. Inoue, T. Takemura, K. Suzuki, M. Kitagawa, IAP family protein expression correlates with poor outcome of multiple myeloma patients in association with chemotherapy-induced overexpression of multidrug resistance genes, Am. J. Hematol. 81 (2006) 824–831. https://doi.org/10.1002/ajh.20656.

[11] H.M. Kluger, M.M. McCarthy, A.B. Alvero, M. Sznol, S. Ariyan, R.L. Camp, D.L. Rimm, G. Mor, The X-linked inhibitor of apoptosis protein (XIAP) is up-regulated in metastatic melanoma, and XIAP cleavage by Phenoxodiol is associated with Carboplatin sensitization, J. Transl. Med. 5 (2007) 1–15. https://doi.org/10.1186/1479-5876-5-6.

[12] C. Chen, T. Wang, F. Wu, W. Huang, G. He, L. Ouyang, M. Xiang, C. Peng, Q. Jiang, Combining structure-based pharmacophore modeling, virtual screening, and in silico ADMET analysis

to discover novel tetrahydro-quinoline based pyruvate kinase isozyme M2 activators with antitumor activity, Drug Des. Devel. Ther. 8 (2014) 1195–1210. https://doi.org/10.2147/DDDT.S62921.

[13] J. Xiao, S. Zhang, M. Luo, Y. Zou, Y. Zhang, Y. Lai, Effective virtual screening strategy focusing on the identification of novel Bruton's tyrosine kinase inhibitors, J. Mol. Graph. Model. 60 (2015) 142–154. https://doi.org/10.1016/j.jmgm.2015.05.005.

[14] S. Vardhan, S.K. Sahoo, In silico ADMET and molecular docking study on searching potential inhibitors from limonoids and triterpenoids for COVID-19, Comput. Biol. Med. 124 (2020) 103936. https://doi.org/10.1016/j.compbiomed.2020.103936.

[15] F.A.D.M. Opo, M.M. Rahman, F. Ahammad, I. Ahmed, M.A. Bhuiyan, A.M. Asiri, Structure-based pharmacophore modeling, virtual screening, molecular docking and ADMET approaches for identification of natural anticancer agents targeting XIAP protein, Sci. Rep. 11 (2021) 1–17. https://doi.org/10.1038/s41598-021-83626-x.

[16] B. Orlikova, D. Tasdemir, F. Golais, M. Dicato, M. Diederich, Dietary chalcones with chemopreventive and chemotherapeutic potential, Genes Nutr. 6 (2011) 125–147. https://doi.org/10.1007/s12263-011-0210-5.

[17] T. Constantinescu, C.N. Lungu, Anticancer activity of natural and synthetic chalcones, Int. J. Mol. Sci. 22 (2021) 1–33. https://doi.org/10.3390/ijms222111306.

[18] T. Seitz, C. Hackl, K. Freese, P. Dietrich, A. Mahli, R.M. Thasler, W.E. Thasler, S.A. Lang, A.K. Bosserhoff, C. Hellerbrand, Xanthohumol, a prenylated chalcone derived from hops, inhibits growth and metastasis of melanoma cells, Cancers (Basel). 13 (2021) 1–12. https://doi.org/10.3390/cancers13030511.

[19] A. Sławińska-Brych, B. Zdzisińska, M. Dmoszyńska-Graniczka, W. Jeleniewicz, J. Kurzepa, M. Gagoś, A. Stepulak, Xanthohumol inhibits the extracellular signal regulated kinase (ERK) signalling pathway and suppresses cell growth of lung adenocarcinoma cells, Toxicology. 357–358 (2016) 65–73. https://doi.org/10.1016/j.tox.2016.06.008.

[20] S.Y. Kim, I.S. Lee, A. Moon, 2-Hydroxychalcone and xanthohumol inhibit invasion of triple negative breast cancer cells, Chem. Biol. Interact. 203 (2013) 565–572. https://doi.org/10.1016/j.cbi.2013.03.012.

[21] Daina, A., Michielin, O., & Zoete, V. (2017). SwissADME: A free web tool to evaluate pharmacokinetics, drug-likeness and medicinal chemistry friendliness of small molecules. Scientific Reports, 7(January), 1–13. https://doi.org/10.1038/srep42717.

[22] Allouche, A. (2012). Software News and Updates Gabedit — A Graphical User Interface for Computational Chemistry Softwares. Journal of Computational Chemistry, 32, 174–182. https://doi.org/10.1002/jcc.

[23] Nikitin, A. M., Milchevskiy, Y. V., & Lyubartsev, A. P. (2014). A new AMBER-compatible force field parameter set for alkanes. Journal of Molecular Modeling, 20(3). https://doi.org/10.1007/s00894-014-2143-6.

[24] Nikitin, A., Milchevskiy, Y., & Lyubartsev, A. (2015). AMBER-II: New Combining Rules and Force Field for Perfluoroalkanes. Journal of Physical Chemistry B, 119(46), 14563–14573. https://doi.org/10.1021/acs.jpcb.5b07233.

[25] Yang, J. M., & Chen, C. C. (2004). GEMDOCK: A Generic Evolutionary Method for Molecular Docking. Proteins: Structure, Function and Genetics, 55(2), 288–304. https://doi.org/10.1002/prot.20035.

[26] Pettersen, E. F., Goddard, T. D., Huang, C. C., Couch, G. S., Greenblatt, D. M., Meng, E. C., & Ferrin, T. E. (2004). UCSF Chimera - A visualization system for exploratory research and analysis. Journal of Computational Chemistry, 25(13), 1605–1612. https://doi.org/10.1002/jcc.20084.

[27] Vlasiou, M. C., & Pafti, K. S. (2021). Screening possible drug molecules for Covid-19. The example of vanadium (III/IV/V) complex molecules with computational chemistry and molecular docking. Computational Toxicology, 18(August 2020). https://doi.org/10.1016/j.comtox.2021.100157.

[28] Vlasiou, M., & Pafiti, K. S. (2022). Dft studies and molecular dynamics of the molecular and electronic structure of cu (Ii) and zn (ii) complexes with the symmetric ligand (z)-2-((3,5-dimethyl-2h-pyrrol-2-yl) methylene)-3,5-dimethyl-2h-pyrrole. Biointerface Research in Applied Chemistry, 12(5), 5953–5968. https://doi.org/10.33263/BRIAC125.59535968.

[29] Vlasiou, M. C. (2021). Structural characterization of two novel, biological active chalcone derivatives, using density functional theory studies. Biointerface Research in Applied Chemistry, 11(6), 15051–15057. https://doi.org/10.33263/BRIAC116.1505115057.

[30] Peiwei You,; Daqiang Chen,; Chao Lian,; Cui Zhang,; Sheng Meng. First-principles dynamics of photoexcited molecules and materials towards a quantum description. WIREs Comput. Mol. Sci. 2021, 11, 1492, https://doi.org/10.1002/wcms.1492.

[31] Zhang, X; Li, Y.; Guo, S.; Zhang, W.; The effects of different substitution heterocycles on ESIPT processes for three 2-(2′-hydroxybenzofuran)-benzoxazole compounds. Chemical Physics 2021, 543, 111081, https://doi.org/10.1016/j.chemphys.2020.111081.

Preprints (www.preprints.org) | NOT PEER-REVIEWED | Posted: 9 June 2022 doi:10.20944/preprints202206.0144.v1

Supplementary Material

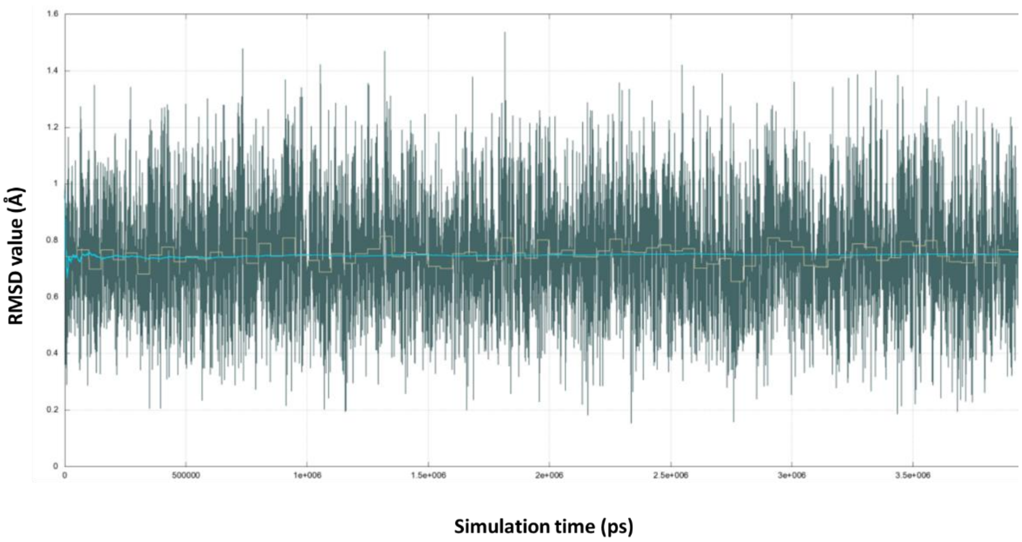

SFigure 1: RMSD value for (E)-1-(4-methoxyphenyl)-3-(p-tolyl) prop-2-en-1-one during simulation time.

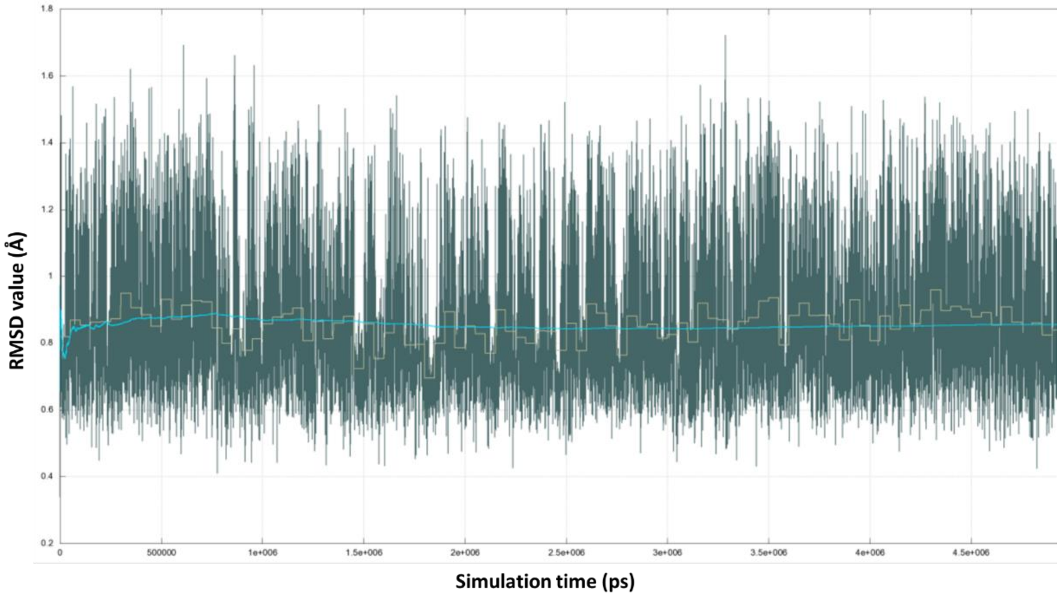

SFigure 2: RMSD value for (E)-3-(4-hydroxyphenyl)-1-(2,4,6-trihydroxyphenyl) prop-2-en-1-one during simulation time.

Preprints (www.preprints.org) | NOT PEER-REVIEWED | Posted: 9 June 2022 doi:10.20944/preprints202206.0144.v1

STable 1: Pharmacophore model.

x	**y**	**z**	**Radius**	**Enabled**
Hydrogen Acceptor	50.3	63.89	7.03	0.5
Hydrogen Acceptor	53.19	67.16	5.08	0.5
Hydrogen Acceptor	53.1	59.29	7.83	0.5
Hydrogen Acceptor	51.05	58.12	13.78	0.5
Hydrogen Acceptor	53.1	59.29	7.83	0.5
Hydrogen Donor	51.05	58.12	13.78	1
Hydrogen Donor	50.1	62.51	7.11	1
Hydrogen Donor	54.32	67.29	4.26	1
Hydrogen Donor	52.78	64.59	6.02	1
Hydrophobic	51.6	59.05	11.23	1